Geophysical Model Function for the AMSR2 C-Band Wind Excess Emissivity at High Winds

Elizaveta V. Zabolotskikh, Nicolas Reul, and Bertrand Chapron

***Abstract*—Measurements of the Advanced Microwave Scanning Radiometer 2 (AMSR2) onboard the Global Change Observation Mission–Water 1 (GCOM-W1) satellite at 6.925 and 7.3 GHz and both linear polarizations over tropical cyclones (TCs) during 2012–2014 are used to derive a new geophysical function relating the brightness temperature to the sea surface wind speed (SWS) in extreme conditions. Similar sensitivity to the SWS at close C-band frequencies allowed correcting for the atmospheric contributions to the microwave radiance and estimating the brightness temperature (T_B) at the surface under TCs, combining theoretical modeling and measured T_B analyses. Estimated oceanic T_B were regressed against the wind speeds from the Best Track Archive to derive a new geophysical model function for the wind speed excess emissivity at AMSR2 C-band microwave frequencies.**

***Index Terms*—Atmosphere, geophysical measurements, oceans, passive microwave remote sensing, tropical cyclones (TCs).**

I. Introduction

REMOTELY sensed measurements from passive and active microwave instruments ensure global wind mapping capabilities. Active microwave copolarized backscatter signals of currently operating instruments saturate under hurricane force winds [1] and are heavily affected in the presence of high rain rates, ensuring an increasing role of microwave radiometry. As it has been established previously [2]–[4], whitecaps, streaks, and various associated foam structures at the ocean surface significantly increase the microwave emissivity of the sea surface. This emissivity increase is observable even when a very small portion of the sea surface is covered by foam formations. As opposed to the scatterometer signal, the radiometric signal does not saturate at high winds, providing the potential for foam property and surface wind speed (SWS) retrievals using passive microwave observations [2], [5]–[7]. Moreover, the sensitivity of microwave brightness temperature tends to even increase for winds above 15 m/s [8]–[10]. Nevertheless, numerical estimations of the wind speed sensitivity at frequencies higher than L-band are essentially complicated by the intervening atmosphere. At C-band and higher frequency bands, atmospheric absorption, emission, and scattering associated with high cloud liquid and ice water content and intense precipitations in tropical cyclones (TCs) have large impacts on the brightness temperatures. Intensive rains both shield the ocean surface and change the ocean surface emissivity in a complicated manner. This influence is hard to be theoretically modeled, particularly for the extreme events combining very high precipitation rate and hurricane force winds. Whereas the microwave radiation at L-band is almost transparent to the atmosphere with negligible impacts of precipitation and water clouds with respect to those reported at higher frequency bands, the L-band ocean emissivity is less sensitive to sea surface state changes at high winds than at the higher C- and X-band microwave frequencies.

The new Japanese passive microwave instrument Advanced Microwave Scanning Radiometer 2 (AMSR2), which was launched in May 2012, has four C-band channels at the frequencies of 6.925 and 7.3 GHz, both on vertical and horizontal polarizations. The two new C-band channel measurements, along with the other C- and X-band measurements, may be explored to estimate the rain radiance and atmospheric transmittance at C-band since the signal at close frequencies has similar sensitivity to the sea SWS but differs in the sensitivity to rain. Such estimation can help in the separation of the ocean signal from the total brightness temperature and in the derivation of the geophysical model function (GMF) that relates the surface excess emissivity and wind speed at the AMSR2 C-band microwave frequencies. In this letter, this GMF is derived through analyses of the AMSR2 brightness temperature (T_B) fields over an ensemble of TCs and through the use of a radiative transfer forward model of T_B.

II. Methodology

Simulation of the microwave brightness temperatures over the oceans as functions of frequency [11]–[13] shows that, at C-band frequencies, the radiative transfer equation (RTE) of the emission type is valid for the rainfall range up to 20 mm/h. In the simplified form, the RTE for the brightness temperature of the atmosphere–ocean system T_B can be written as

$$\cos\theta \cdot \frac{dT_B}{dz} = -\alpha(z)T_B + \alpha(z)T(z) \quad (1)$$

where θ is the incidence angle, and $T(z)$ is the vertical profile of the atmospheric temperature. This "absorption only" form

Manuscript received September 22, 2015; revised October 13, 2015; accepted October 27, 2015. This work was supported in part by the Ministry of Education and Science of the Russian Federation under Project RFMEFI58615X0017 and in part by the European Space Agency Support to Science through the Soil Moisture and Ocean Salinity (SMOS)+Storm Evolution Project.

E. V. Zabolotskikh is with the Satellite Oceanography Laboratory, Russian State Hydrometeorological University, St. Petersburg 195196, Russia (e-mail: liza@rshu.ru).

N. Reul and B. Chapron are with Institut Francais de Recherche et d'Exploitation de la Mer, 29280 Plouzané, France (e-mail: nreul@ifremer.fr; bchapron@ifremer.fr).

Color versions of one or more of the figures in this paper are available online at http://ieeexplore.ieee.org.

Digital Object Identifier 10.1109/LGRS.2015.2497463

1545-598X © 2015 IEEE. Personal use is permitted, but republication/redistribution requires IEEE permission.
See http://www.ieee.org/publications_standards/publications/rights/index.html for more information.

IEEE Proof

of the RTE, where absorption coefficient $\alpha_{\mathrm{absorption}}(z)$ is replaced by total attenuation coefficient $\alpha(z)$, accounts accurately for the negative effect of scattering and approximately for its positive effect due to the forward scattering [14]. Note that it does not account for the polarization effect of scattering that increases with the rain rate.

The solution of (1) can be written as

$$T_B = T_a + T_a \cdot (1-\varepsilon) \cdot \exp(-\tau) + T_S \cdot \varepsilon \cdot \exp(-\tau) + T_c \tag{2}$$

where T_a is the radiation of the atmosphere, which in (2) is supposed to be equal in its upwelling and downwelling parts [15]; ε is the sea surface emissivity, which is strongly dependent on the sea SWS; τ is the atmospheric optical thickness; and T_S is the sea surface temperature (SST). Cosmic radiation T_c can be written as $T_c = 2.73 \cdot \exp(-2\tau) \cdot (1-\varepsilon)$ [16].

To further simplify (2), we express T_a as $T_{\mathrm{eff}}\ \tau$, where T_{eff} is the effective atmospheric temperature [15], and replace $\exp(-\tau)$ by $(1-\tau)$ according to the Taylor approximation. For nonprecipitating atmospheres, the error of this approximation is less than 0.1% for C-band frequencies. At $\tau \sim 0.3$ (corresponding at C-band to high rain rates), the error of such an approximation is about 5%. Considering T_c to be less than 2 K for horizontal polarization and less than 1.3 K for vertical polarization (maximum T_c values for calm sea surface and transparent atmospheres), we excluded the cosmic radiation from the following consideration. After these simplifications, (2) can be written as

$$T_B \approx T_{\mathrm{eff}} \cdot \tau + T_{\mathrm{eff}} \cdot \tau \cdot (1-\varepsilon) \cdot (1-\tau) + T_S \cdot \varepsilon \cdot (1-\tau). \tag{3}$$

Thus, sea surface emissivity ε can be calculated through the following expression:

$$\varepsilon \approx \frac{T_B - T_{\mathrm{eff}} \cdot \tau \cdot (2-\tau)}{(T_S - T_{\mathrm{eff}} \cdot \tau) \cdot (1-\tau)}. \tag{4}$$

Knowing T_B, T_S, τ, and T_{eff}, we can calculate ε and relate it to the sea SWS to derive the GMF for wind speed dependence.

To parameterize T_{eff}, we used numerical calculations of the atmospheric contribution to the brightness temperature. An input data set of about 7000 radiosounding profiles from the tropical radiosounding stations, which was complemented by the model profiles of liquid water content and the rain rate, was used. The clear-sky atmospheric radiation was evaluated using widely used and intensively validated models, e.g., see [17] for molecular oxygen and [18] for water vapor absorption. Liquid water content absorption and rain rate attenuation were calculated using the parameterization of the work in [17]. Fig. 1 shows the dependence of T_a on the atmospheric attenuation at 6.9 GHz $\tau_{6.9}$ for the whole data set of the atmospheric parameter profiles. With some degree of accuracy, we can define T_{eff} as a constant of 260 K in (4). Numerical calculations also allow to express the atmospheric attenuation at 6.9 GHz as a function of the atmospheric attenuation at 10.65 GHz $\tau_{10.65}$, i.e., $\tau_{6.9} \approx 0.87 \cdot \tau_{10.65}$. The atmospheric attenuation at 10.65 GHz can be presented as a sum of the atmospheric absorption τ_0 of the system without rain, which can be estimated

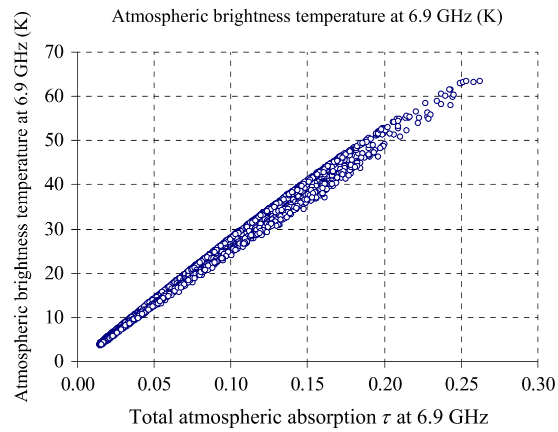

Fig. 1. Atmospheric brightness temperature T_a at 6.9 GHz as a function of total atmospheric absorption $\tau_{6.9}$.

using the approach described in [19], and the attenuation of rain τ_R, i.e.,

$$\tau_R = 0.0038 \cdot T_R. \tag{5}$$

Equation (5) is the regression result of the numerical simulations, where T_R is the rain brightness temperature. In turn, T_R can be separated from the brightness temperature of the atmosphere–ocean system encountered over a TC using the method developed in [20]. Thus, reformulating (4) in terms of the brightness temperature functions, we can write

$$\varepsilon_{6.9} = \frac{T_{B6.9} - 260 \cdot 0.87 \cdot \tau_{10.65} \cdot (2 - 0.87 \cdot \tau_{10.65})}{(T_S - 260 \cdot 0.87 \cdot \tau_{10.65}) \cdot (1 - 0.87 \cdot \tau_{10.65})} \tag{6}$$

where

$$\tau_{10.65} = \tau_0 + 0.0038 \cdot T_R. \tag{7}$$

Using AMSR2 measurements as inputs and applying formulas (6) and (7), we calculated ocean emissivity ε at 6.9 GHz at both horizontal and vertical polarizations. τ_0 was calculated using the measurements at 10.65, 18.7, and 23.8 GHz at both horizontal and vertical polarizations for which the neural network algorithm described in [19] was applied. T_R was calculated using the differences in the measurements between the C- and X-band channels at vertical polarization, as described in [20]. The SST daily satellite product described hereafter was used as a source for the SST data.

III. Data

The TC information (Best Track Data) for 2012–2014 (years of the AMSR2 available data) was downloaded from the National Hurricane Center for the North Atlantic and Northeast Pacific TCs and from the Japan Meteorological Agency (JMA) (Regional Specialized Meteorological Center Tokyo–Typhoon Center) for the Northwest TCs (http://agora.ex.nii.ac.jp/digital-typhoon).

AMSR2 Level-1B swath brightness temperature data were downloaded from the Global Change Observation Mission–Water 1 (GCOM-W1) Data Providing Service, Japan

IEEE Proof

Aerospace Exploration Agency. AMSR2 Level-1B T_B data at C- and X-band channels are provided on the same irregular grid of 10 km $\times$ 10 km [21], which simplifies the use of the data at different channels in the equations for the ocean emission calculations.

We used the 9-km microwave plus infrared (MW_IR) optimally interpolated (OI) SST product downloaded from the Remote Sensing Systems website to characterize the fields of SST T_S (ftp://data.remss.com/SST/\ignorespacesdaily_v04.0/mw_ir/).

For the numerical calculations that allowed to parameterize $T_a = 260 \cdot \tau_{6.9}$, $\tau_{6.9} = 0.87 \cdot \tau_{10.65}$, and $\tau_R = 0.0038 \cdot T_R$, we used the data set of about 7000 radiosounding profiles of air temperature, humidity, and pressure from the tropical weather stations, which was collected by the University of Wyoming. This data set consists of cloud liquid water content profiles, which are modeled in accordance with the work in [22]. For those data that exhibited modeled total liquid water content less than 0.3 kg/m^2, we assumed an absence of rain drops. For cloudy conditions, which were characterized by the total liquid water content exceeding 0.3 kg/m^2, uniformly distributed point rain rates were randomly added with a rain rate from 0 up to 20 mm/h within the rain depth of 0.5–4.5 km, depending on the humidity and temperature profiles.

IV. Results

Using AMSR2 measurements, the SST OI MW_IR product, and the equations provided earlier, we estimated ocean emissivity ε at 6.9 GHz at both horizontal and vertical polarizations. The fields of ocean emissivity ε at 6.9 GHz at both horizontal and vertical polarizations were built for 110 North Atlantic and North Pacific TCs intercepted by AMSR2 swath over the period from 2012 to 2014. About 600 full intercepts were analyzed to match the maximum values of ε over the TCs with the maximum 1-min sustained SWS estimates from the Best Track Archives, which were downscaled with a factor ranging from 0.93- [23] to 10-min winds to correspond to the AMSR2 spatial resolution. The new GMF at both vertical and horizontal polarizations for the microwave C-band emission at high winds in TCs was then obtained by relating $\varepsilon_{\max}$ at 6.9 GHz and the maximum sustained wind $\mathrm{SWS}_{\max}$.

An example of the fields of the calculated ocean radiances at 6.9 GHz, horizontal polarization $\Delta T_{Bocean}{}^H = \varepsilon^H \cdot T_S$ and at 6.9 GHz, vertical polarization $\Delta T_{Bocean}{}^V = \varepsilon^V \cdot T_S$ over the Typhoon Danas in the West Pacific Ocean on October 7, 2013 at $\sim$17:00 Coordinated Universal Time (UTC) is presented in Fig. 2. The coordinate system is linked to the center of the cyclone, which is found by the Best Track Data interpolation for the measurement time. The vertical axis corresponds to the storm translation movement direction (along track), and the distances are given in kilometers from the center of the cyclone. The masked (white) pixels in Fig. 2 indicate land and coastal zones. For that particular example, the maximum values of the wind-induced excess brightness temperature were of $\Delta T_{Bocean}{}^H = 108$ K and $\Delta T_{Bocean}{}^V = 185$ K in H and V polarizations, respectively. The surface temperature was $T_S = 295$ K, and the maximum value of the 1-min wind speed, which

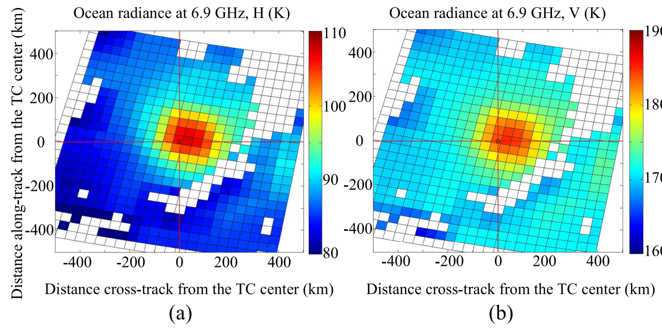

Fig. 2. Fields of the calculated ocean radiances at (a) 6.9 GHz, horizontal polarization $\Delta T_{Bocean}{}^H$ and at (b) 6.9 GHz, vertical polarization $\Delta T_{Bocean}{}^V$ over the TC Danas in the West Pacific Ocean on October 7, 2013 at $\sim$17:00 UTC. The center of the cyclone is found by the Best Track Data interpolation for the measurement time.

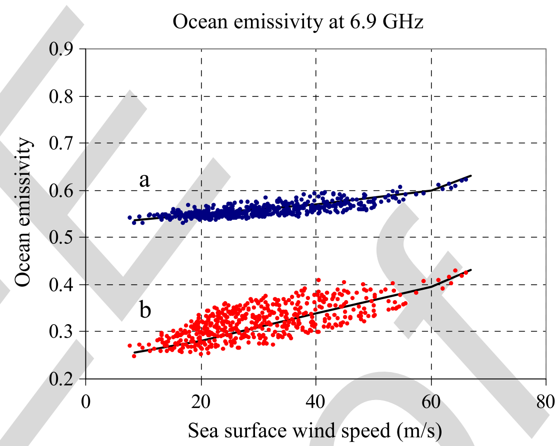

Fig. 3. Maximum values of the ocean emissivities at 6.9 GHz at (a) horizontal and (b) vertical polarizations for about 600 AMSR2 intercepts of the North Atlantic and North Pacific TCs, which were calculated using (6) and (7) as functions of the 10-min maximum sea SWS, taken from the Best Track Data.

is taken from the Best Track Data Archive of JMA, is reported to be 40 m/s at 18:00 UTC that corresponds to 37.2 m/s of 10-min wind. Therefore, for ε^H at 37.2 m/s, we have the value of $105/295 = 0.37$, and for ε^V at 37.2 m/s, we have the value of $182/295 = 0.63$.

The derived ocean emissivities at 6.9 GHz at horizontal and vertical polarizations following such methodology for about 600 AMSR2 intercepts of North Atlantic and North Pacific TCs were collected and are plotted as a function of the 10-min SWS in Fig. 3.

Since the scatter of the data is quite large both for vertically polarized and horizontally polarized signals, the equations for the interpolation curves cannot be derived unambiguously. Analyzing Fig. 3, we would suggest separating the SWS range to several ranges and calculating the radiance sensitivity as a linear function for every range. The corresponding ocean brightness temperature sensitivities to the SWS for several SWS ranges are presented in Table I.

Up to 15 m/s, the sensitivity slowly grows with the SWS for both polarizations, with horizontal polarization being almost twice more sensitive to wind speed than vertical polarization. As the wind speed exceeds 15 m/s, the slopes steadily increase

IEEE Proof

TABLE I
OCEAN BRIGHTNESS TEMPERATURE SENSITIVITIES TO THE SEA SWS

SWS, m/s	ΔT_{Bocean}^{H}, K/(m/s)	ΔT_{Bocean}^{V}, K/(m/s)
< 15	0.4	0.2
15 - 20	0.6	0.3
20 - 40	0.8	0.4
40 - 60	1.0	0.5
> 60	1.5	1.3

from 0.27 up to 0.38 for horizontal polarization and from 0.54 up to 0.6 for vertical polarization, with a sharp rise at extremely high winds higher than 55–60 m/s. These values are about 1.5 times lower than those given by the empirical model from the work in [24].

REFERENCES

[1] W. J. Donnelly *et al.*, "Revised ocean backscatter models at C and Ku band under high-wind conditions," *J. Geophys. Res. Oceans*, vol. 104, no. C5, pp. 11 485–11 497, May 1999.

[2] N. Reul and B. Chapron, "A model of sea-foam thickness distribution for passive microwave remote sensing applications," *J. Geophys. Res. Oceans*, vol. 108, no. C10, pp. 1–14, Oct. 2003.

[3] A. Stogryn, "The emissivity of sea foam at microwave frequencies," *J. Geophys. Res.*, vol. 77, no. 9, pp. 1658–1666, Mar. 1972.

[4] M. D. Anguelova and P. W. Gaiser, "Dielectric and radiative properties of sea foam at microwave frequencies: Conceptual understanding of foam emissivity," *Remote Sens.*, vol. 4, no. 5, pp. 1162–1189, Apr. 2012.

[5] Y. Quilfen, C. Prigent, B. Chapron, A. A. Mouche, and N. Houti, "The potential of QuikSCAT and WindSat observations for the estimation of sea surface wind vector under severe weather conditions," *J. Geophys. Res.*, vol. 112, no. C9, Sep. 2007, Art. ID 01480227.

[6] N. Reul *et al.*, "SMOS satellite L-band radiometer: A new capability for ocean surface remote sensing in hurricanes," *J. Geophys. Res. Oceans*, vol. 117, no. C2, pp. 1–24, Feb. 2012.

[7] L. H. Holthuijsen, M. D. Powell, and J. D. Pietrzak, "Wind and waves in extreme hurricanes," *J. Geophys. Res. Oceans*, vol. 117, no. C9, pp. 1–15, Sep. 2012.

[8] S. Soisuvarn, Z. Jelenak, and W. L. Jones, "An ocean surface wind vector model function for a spaceborne microwave radiometer," *IEEE Trans. Geosci. Remote Sens.*, vol. 45, no. 10, pp. 3119–3130, Oct. 2007.

[9] E. W. Uhlhorn *et al.*, "Hurricane surface wind measurements from an operational stepped frequency microwave radiometer," *Monthly Weather Rev.*, vol. 135, no. 9, pp. 3070–3085, Sep. 2007.

[10] T. Meissner and F. J. Wentz, "The emissivity of the ocean surface between 6 and 90 GHz over a large range of wind speeds and earth incidence angles," *IEEE Trans. Geosci. Remote Sens.*, vol. 50, no. 8, pp. 3004–3026, Aug. 2012.

[11] F. J. Wentz, "A model function for ocean microwave brightness temperatures," *J. Geophys. Res.*, vol. 88, no. C3, pp. 1892–1908, Feb. 1983.

[12] C. Kummerow and R. Ferraro, *Algorithm Theoretical Basis Document: EOS/AMSR-E Level-2 Rainfall*. Fort Collins, CO, USA: Colorado State Univ. Rep., 2007, pp. 1–10.

[13] C. Surussavadee and D. H. Staelin, "Millimeter-wave precipitation retrievals and observed-versus-simulated radiance distributions: Sensitivity to assumptions," *J. Atmos. Sci.*, vol. 64, no. 11, pp. 3808–3826, Nov. 2007.

[14] S. Y. Matrosov and E. M. Shulgina, "Scattering and attenuation of microwave radiation by precipitation," *MGO Trans.*, vol. 448, pp. 85–94, 1982.

[15] L. M. Mitnik and M. L. Mitnik, "Retrieval of atmospheric and ocean surface parameters from ADEOS-II Advanced Microwave Scanning Radiometer (AMSR) data: Comparison of errors of global and regional algorithms," *Radio Sci.*, vol. 38, no. 4, p. 8065, Aug. 2003.

[16] F. J. Wentz, "A well-calibrated ocean algorithm for special sensor microwave/imager," *J. Geophys. Res.*, vol. 102, no. C4, pp. 8703–8718, Apr. 1997.

[17] H. J. Liebe and D. H. Layton, "Millimeter-wave properties of the atmosphere: Laboratory studies and propagation modeling," Nat. Tech. Inf. Serv. Boulder, CO, USA, NTIA Rep. 87-24, 1987.

[18] D. D. Turner, M. P. Cadeddu, U. Lohnert, S. Crewell, and A. M. Vogelmann, "Modifications to the water vapor continuum in the microwave suggested by ground-based 150-GHz observations," *IEEE Trans. Geosci. Remote Sens. Lett.*, vol. 47, no. 10, pp. 3326–3337, Oct. 2009.

[19] E. V. Zabolotskikh, L. M. Mitnik, and B. Chapron, "New approach for severe marine weather study using satellite passive microwave sensing," *Geophys. Res. Lett.*, vol. 40, no. 13, pp. 3347–3350, Jul. 2013.

[20] E. Zabolotskikh, L. Mitnik, N. Reul, and B. Chapron, "New possibilities for geophysical parameter retrievals opened by GCOM-W1 AMSR2," *IEEE J. Sel. Topics Appl. Earth Observ. Remote Sens.*, to be published. **AQ2**

[21] GCOM-W1 Data Providing Service Users Manual Jpn Aerosp. Exploration Agency, Tokyo, Japan, 2013.

[22] I. P. Mazin and A. K. Khrgian, *Clouds and Cloudy Atmosphere*. Leningrad, Russia: Gidrometeoizdat, 1989.

[23] B. A. Harper, J. D. Kepert, and J. D. Ginger, "Guidelines for converting between various wind averaging periods in tropical cyclone conditions," World Meteorol. Org. TCP Sub-Project Rep., Geneva, Switzerland, 1555, 2010.

[24] B. Chapron *et al.*, "Ocean remote sensing data integration-examples and outlook," in *Proc. OceanObs*, 2010, pp. 1–11.

IEEE Proof

AUTHOR QUERIES

AUTHOR PLEASE ANSWER ALL QUERIES

Please be aware that authors are required to pay overlength page charges ($200 per page) if the paper is longer than 3 pages. If you cannot pay any or all of these charges please let us know.

This pdf contains 2 proofs. The first half is the version that will appear on Xplore. The second half is the version that will appear in print. If you have any figures to print in color, they will be in color in both proofs.

The "Open Access" option for your paper expires when the paper is published on Xplore in an issue with page numbers. Papers in "Early Access" may be changed to "Open Access."

AQ1 = Please check if the provided definition for GCOM-W1 here in the abstract and in the body of the text is correct, and please amend if necessary.
AQ2 = Please provide publication update in Ref. [20].

END OF ALL QUERIES

IEEE Proof

Geophysical Model Function for the AMSR2 C-Band Wind Excess Emissivity at High Winds

Elizaveta V. Zabolotskikh, Nicolas Reul, and Bertrand Chapron

***Abstract*—Measurements of the Advanced Microwave Scanning Radiometer 2 (AMSR2) onboard the Global Change Observation Mission–Water 1 (GCOM-W1) satellite at 6.925 and 7.3 GHz and both linear polarizations over tropical cyclones (TCs) during 2012–2014 are used to derive a new geophysical function relating the brightness temperature to the sea surface wind speed (SWS) in extreme conditions. Similar sensitivity to the SWS at close C-band frequencies allowed correcting for the atmospheric contributions to the microwave radiance and estimating the brightness temperature (T_B) at the surface under TCs, combining theoretical modeling and measured T_B analyses. Estimated oceanic T_B were regressed against the wind speeds from the Best Track Archive to derive a new geophysical model function for the wind speed excess emissivity at AMSR2 C-band microwave frequencies.**

***Index Terms*—Atmosphere, geophysical measurements, oceans, passive microwave remote sensing, tropical cyclones (TCs).**

I. Introduction

REMOTELY sensed measurements from passive and active microwave instruments ensure global wind mapping capabilities. Active microwave copolarized backscatter signals of currently operating instruments saturate under hurricane force winds [1] and are heavily affected in the presence of high rain rates, ensuring an increasing role of microwave radiometry. As it has been established previously [2]–[4], whitecaps, streaks, and various associated foam structures at the ocean surface significantly increase the microwave emissivity of the sea surface. This emissivity increase is observable even when a very small portion of the sea surface is covered by foam formations. As opposed to the scatterometer signal, the radiometric signal does not saturate at high winds, providing the potential for foam property and surface wind speed (SWS) retrievals using passive microwave observations [2], [5]–[7]. Moreover, the sensitivity of microwave brightness temperature tends to even increase for winds above 15 m/s [8]–[10]. Nevertheless, numerical estimations of the wind speed sensitivity at frequencies higher than L-band are essentially complicated by the intervening atmosphere. At C-band and higher frequency bands, atmospheric absorption, emission, and scattering associated with high cloud liquid and ice water content and intense precipitations in tropical cyclones (TCs) have large impacts on the brightness temperatures. Intensive rains both shield the ocean surface and change the ocean surface emissivity in a complicated manner. This influence is hard to be theoretically modeled, particularly for the extreme events combining very high precipitation rate and hurricane force winds. Whereas the microwave radiation at L-band is almost transparent to the atmosphere with negligible impacts of precipitation and water clouds with respect to those reported at higher frequency bands, the L-band ocean emissivity is less sensitive to sea surface state changes at high winds than at the higher C- and X-band microwave frequencies.

The new Japanese passive microwave instrument Advanced Microwave Scanning Radiometer 2 (AMSR2), which was launched in May 2012, has four C-band channels at the frequencies of 6.925 and 7.3 GHz, both on vertical and horizontal polarizations. The two new C-band channel measurements, along with the other C- and X-band measurements, may be explored to estimate the rain radiance and atmospheric transmittance at C-band since the signal at close frequencies has similar sensitivity to the sea SWS but differs in the sensitivity to rain. Such estimation can help in the separation of the ocean signal from the total brightness temperature and in the derivation of the geophysical model function (GMF) that relates the surface excess emissivity and wind speed at the AMSR2 C-band microwave frequencies. In this letter, this GMF is derived through analyses of the AMSR2 brightness temperature (T_B) fields over an ensemble of TCs and through the use of a radiative transfer forward model of T_B.

II. Methodology

Simulation of the microwave brightness temperatures over the oceans as functions of frequency [11]–[13] shows that, at C-band frequencies, the radiative transfer equation (RTE) of the emission type is valid for the rainfall range up to 20 mm/h. In the simplified form, the RTE for the brightness temperature of the atmosphere–ocean system T_B can be written as

$$\cos\theta \cdot \frac{dT_B}{dz} = -\alpha(z)T_B + \alpha(z)T(z) \qquad (1)$$

where θ is the incidence angle, and $T(z)$ is the vertical profile of the atmospheric temperature. This "absorption only" form

Manuscript received September 22, 2015; revised October 13, 2015; accepted October 27, 2015. This work was supported in part by the Ministry of Education and Science of the Russian Federation under Project RFMEFI58615X0017 and in part by the European Space Agency Support to Science through the Soil Moisture and Ocean Salinity (SMOS)+Storm Evolution Project.

E. V. Zabolotskikh is with the Satellite Oceanography Laboratory, Russian State Hydrometeorological University, St. Petersburg 195196, Russia (e-mail: liza@rshu.ru).

N. Reul and B. Chapron are with Institut Francais de Recherche et d'Exploitation de la Mer, 29280 Plouzané, France (e-mail: nreul@ifremer.fr; bchapron@ifremer.fr).

Color versions of one or more of the figures in this paper are available online at http://ieeexplore.ieee.org.

Digital Object Identifier 10.1109/LGRS.2015.2497463

1545-598X © 2015 IEEE. Personal use is permitted, but republication/redistribution requires IEEE permission.
See http://www.ieee.org/publications_standards/publications/rights/index.html for more information.

IEEE Proof

of the RTE, where absorption coefficient $\alpha_{\mathrm{absorption}}(z)$ is replaced by total attenuation coefficient $\alpha(z)$, accounts accurately for the negative effect of scattering and approximately for its positive effect due to the forward scattering [14]. Note that it does not account for the polarization effect of scattering that increases with the rain rate.

The solution of (1) can be written as

$$T_B = T_a + T_a \cdot (1-\varepsilon) \cdot \exp(-\tau) + T_S \cdot \varepsilon \cdot \exp(-\tau) + T_c \tag{2}$$

where T_a is the radiation of the atmosphere, which in (2) is supposed to be equal in its upwelling and downwelling parts [15]; ε is the sea surface emissivity, which is strongly dependent on the sea SWS; τ is the atmospheric optical thickness; and T_S is the sea surface temperature (SST). Cosmic radiation T_c can be written as $T_c = 2.73 \cdot \exp(-2\tau) \cdot (1-\varepsilon)$ [16].

To further simplify (2), we express T_a as $T_{\mathrm{eff}}\ \tau$, where T_{eff} is the effective atmospheric temperature [15], and replace $\exp(-\tau)$ by $(1-\tau)$ according to the Taylor approximation. For nonprecipitating atmospheres, the error of this approximation is less than 0.1% for C-band frequencies. At $\tau \sim 0.3$ (corresponding at C-band to high rain rates), the error of such an approximation is about 5%. Considering T_c to be less than 2 K for horizontal polarization and less than 1.3 K for vertical polarization (maximum T_c values for calm sea surface and transparent atmospheres), we excluded the cosmic radiation from the following consideration. After these simplifications, (2) can be written as

$$T_B \approx T_{\mathrm{eff}} \cdot \tau + T_{\mathrm{eff}} \cdot \tau \cdot (1-\varepsilon) \cdot (1-\tau) + T_S \cdot \varepsilon \cdot (1-\tau). \tag{3}$$

Thus, sea surface emissivity ε can be calculated through the following expression:

$$\varepsilon \approx \frac{T_B - T_{\mathrm{eff}} \cdot \tau \cdot (2-\tau)}{(T_S - T_{\mathrm{eff}} \cdot \tau) \cdot (1-\tau)}. \tag{4}$$

Knowing T_B, T_S, τ, and T_{eff}, we can calculate ε and relate it to the sea SWS to derive the GMF for wind speed dependence.

To parameterize T_{eff}, we used numerical calculations of the atmospheric contribution to the brightness temperature. An input data set of about 7000 radiosounding profiles from the tropical radiosounding stations, which was complemented by the model profiles of liquid water content and the rain rate, was used. The clear-sky atmospheric radiation was evaluated using widely used and intensively validated models, e.g., see [17] for molecular oxygen and [18] for water vapor absorption. Liquid water content absorption and rain rate attenuation were calculated using the parameterization of the work in [17]. Fig. 1 shows the dependence of T_a on the atmospheric attenuation at 6.9 GHz $\tau_{6.9}$ for the whole data set of the atmospheric parameter profiles. With some degree of accuracy, we can define T_{eff} as a constant of 260 K in (4). Numerical calculations also allow to express the atmospheric attenuation at 6.9 GHz as a function of the atmospheric attenuation at 10.65 GHz $\tau_{10.65}$, i.e., $\tau_{6.9} \approx 0.87 \cdot \tau_{10.65}$. The atmospheric attenuation at 10.65 GHz can be presented as a sum of the atmospheric absorption τ_0 of the system without rain, which can be estimated

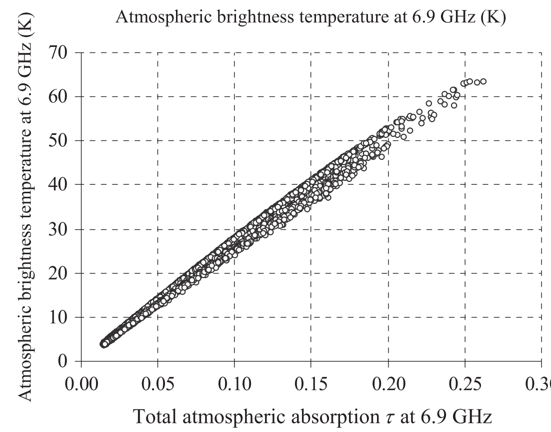

Fig. 1. Atmospheric brightness temperature T_a at 6.9 GHz as a function of total atmospheric absorption $\tau_{6.9}$.

using the approach described in [19], and the attenuation of rain τ_R, i.e.,

$$\tau_R = 0.0038 \cdot T_R. \tag{5}$$

Equation (5) is the regression result of the numerical simulations, where T_R is the rain brightness temperature. In turn, T_R can be separated from the brightness temperature of the atmosphere–ocean system encountered over a TC using the method developed in [20]. Thus, reformulating (4) in terms of the brightness temperature functions, we can write

$$\varepsilon_{6.9} = \frac{T_{B6.9} - 260 \cdot 0.87 \cdot \tau_{10.65} \cdot (2 - 0.87 \cdot \tau_{10.65})}{(T_S - 260 \cdot 0.87 \cdot \tau_{10.65}) \cdot (1 - 0.87 \cdot \tau_{10.65})} \tag{6}$$

where

$$\tau_{10.65} = \tau_0 + 0.0038 \cdot T_R. \tag{7}$$

Using AMSR2 measurements as inputs and applying formulas (6) and (7), we calculated ocean emissivity ε at 6.9 GHz at both horizontal and vertical polarizations. τ_0 was calculated using the measurements at 10.65, 18.7, and 23.8 GHz at both horizontal and vertical polarizations for which the neural network algorithm described in [19] was applied. T_R was calculated using the differences in the measurements between the C- and X-band channels at vertical polarization, as described in [20]. The SST daily satellite product described hereafter was used as a source for the SST data.

III. Data

The TC information (Best Track Data) for 2012–2014 (years of the AMSR2 available data) was downloaded from the National Hurricane Center for the North Atlantic and Northeast Pacific TCs and from the Japan Meteorological Agency (JMA) (Regional Specialized Meteorological Center Tokyo–Typhoon Center) for the Northwest TCs (http://agora.ex.nii.ac.jp/digital-typhoon).

AMSR2 Level-1B swath brightness temperature data were downloaded from the Global Change Observation Mission–Water 1 (GCOM-W1) Data Providing Service, Japan

IEEE Proof

Aerospace Exploration Agency. AMSR2 Level-1B T_B data at C- and X-band channels are provided on the same irregular grid of 10 km $\times$ 10 km [21], which simplifies the use of the data at different channels in the equations for the ocean emission calculations.

We used the 9-km microwave plus infrared (MW_IR) optimally interpolated (OI) SST product downloaded from the Remote Sensing Systems website to characterize the fields of SST T_S (ftp://data.remss.com/SST/\ignorespacesdaily_v04.0/mw_ir/).

For the numerical calculations that allowed to parameterize $T_a = 260 \cdot \tau_{6.9}, \tau_{6.9} = 0.87 \cdot \tau_{10.65}$, and $\tau_R = 0.0038 \cdot T_R$, we used the data set of about 7000 radiosounding profiles of air temperature, humidity, and pressure from the tropical weather stations, which was collected by the University of Wyoming. This data set consists of cloud liquid water content profiles, which are modeled in accordance with the work in [22]. For those data that exhibited modeled total liquid water content less than 0.3 kg/m^2, we assumed an absence of rain drops. For cloudy conditions, which were characterized by the total liquid water content exceeding 0.3 kg/m^2, uniformly distributed point rain rates were randomly added with a rain rate from 0 up to 20 mm/h within the rain depth of 0.5–4.5 km, depending on the humidity and temperature profiles.

IV. RESULTS

Using AMSR2 measurements, the SST OI MW_IR product, and the equations provided earlier, we estimated ocean emissivity ε at 6.9 GHz at both horizontal and vertical polarizations. The fields of ocean emissivity ε at 6.9 GHz at both horizontal and vertical polarizations were built for 110 North Atlantic and North Pacific TCs intercepted by AMSR2 swath over the period from 2012 to 2014. About 600 full intercepts were analyzed to match the maximum values of ε over the TCs with the maximum 1-min sustained SWS estimates from the Best Track Archives, which were downscaled with a factor ranging from 0.93- [23] to 10-min winds to correspond to the AMSR2 spatial resolution. The new GMF at both vertical and horizontal polarizations for the microwave C-band emission at high winds in TCs was then obtained by relating $\varepsilon_{\max}$ at 6.9 GHz and the maximum sustained wind $\mathrm{SWS}_{\max}$.

An example of the fields of the calculated ocean radiances at 6.9 GHz, horizontal polarization $\Delta T_{B\text{ocean}}{}^H = \varepsilon^H \cdot T_S$ and at 6.9 GHz, vertical polarization $\Delta T_{B\text{ocean}}{}^V = \varepsilon^V \cdot T_S$ over the Typhoon Danas in the West Pacific Ocean on October 7, 2013 at $\sim$17:00 Coordinated Universal Time (UTC) is presented in Fig. 2. The coordinate system is linked to the center of the cyclone, which is found by the Best Track Data interpolation for the measurement time. The vertical axis corresponds to the storm translation movement direction (along track), and the distances are given in kilometers from the center of the cyclone. The masked (white) pixels in Fig. 2 indicate land and coastal zones. For that particular example, the maximum values of the wind-induced excess brightness temperature were of $\Delta T_{B\text{ocean}}{}^H = 108$ K and $\Delta T_{B\text{ocean}}{}^V = 185$ K in H and V polarizations, respectively. The surface temperature was $T_S = 295$ K, and the maximum value of the 1-min wind speed, which

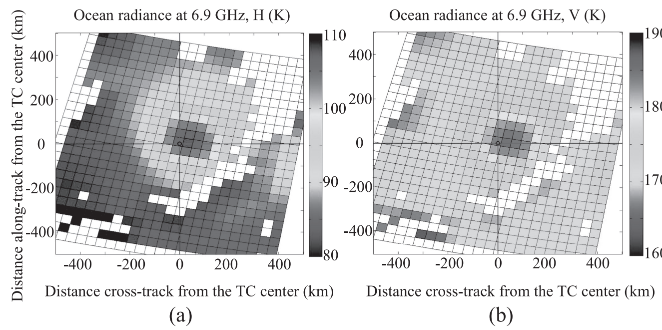

Fig. 2. Fields of the calculated ocean radiances at (a) 6.9 GHz, horizontal polarization $\Delta T_{B\text{ocean}}{}^H$ and at (b) 6.9 GHz, vertical polarization $\Delta T_{B\text{ocean}}{}^V$ over the TC Danas in the West Pacific Ocean on October 7, 2013 at $\sim$17:00 UTC. The center of the cyclone is found by the Best Track Data interpolation for the measurement time.

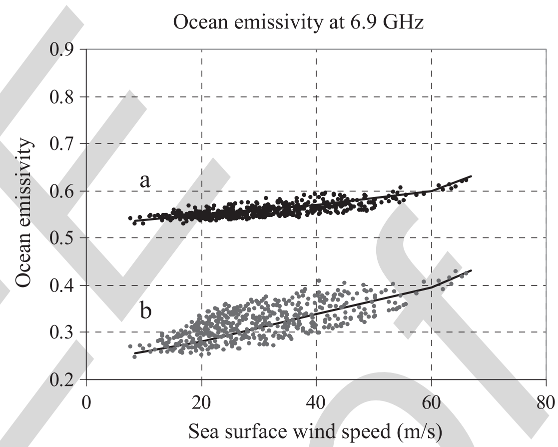

Fig. 3. Maximum values of the ocean emissivities at 6.9 GHz at (a) horizontal and (b) vertical polarizations for about 600 AMSR2 intercepts of the North Atlantic and North Pacific TCs, which were calculated using (6) and (7) as functions of the 10-min maximum sea SWS, taken from the Best Track Data.

is taken from the Best Track Data Archive of JMA, is reported to be 40 m/s at 18:00 UTC that corresponds to 37.2 m/s of 10-min wind. Therefore, for ε^H at 37.2 m/s, we have the value of $105/295 = 0.37$, and for ε^V at 37.2 m/s, we have the value of $182/295 = 0.63$.

The derived ocean emissivities at 6.9 GHz at horizontal and vertical polarizations following such methodology for about 600 AMSR2 intercepts of North Atlantic and North Pacific TCs were collected and are plotted as a function of the 10-min SWS in Fig. 3.

Since the scatter of the data is quite large both for vertically polarized and horizontally polarized signals, the equations for the interpolation curves cannot be derived unambiguously. Analyzing Fig. 3, we would suggest separating the SWS range to several ranges and calculating the radiance sensitivity as a linear function for every range. The corresponding ocean brightness temperature sensitivities to the SWS for several SWS ranges are presented in Table I.

Up to 15 m/s, the sensitivity slowly grows with the SWS for both polarizations, with horizontal polarization being almost twice more sensitive to wind speed than vertical polarization. As the wind speed exceeds 15 m/s, the slopes steadily increase

IEEE Proof

TABLE I
OCEAN BRIGHTNESS TEMPERATURE SENSITIVITIES TO THE SEA SWS

SWS, m/s	ΔT_{Bocean}^{H}, K/(m/s)	ΔT_{Bocean}^{V}, K/(m/s)
< 15	0.4	0.2
15 - 20	0.6	0.3
20 - 40	0.8	0.4
40 - 60	1.0	0.5
> 60	1.5	1.3

from 0.27 up to 0.38 for horizontal polarization and from 0.54 up to 0.6 for vertical polarization, with a sharp rise at extremely high winds higher than 55–60 m/s. These values are about 1.5 times lower than those given by the empirical model from the work in [24].

REFERENCES

[1] W. J. Donnelly *et al.*, “Revised ocean backscatter models at C and Ku band under high-wind conditions,” *J. Geophys. Res. Oceans*, vol. 104, no. C5, pp. 11 485–11 497, May 1999.

[2] N. Reul and B. Chapron, “A model of sea-foam thickness distribution for passive microwave remote sensing applications,” *J. Geophys. Res. Oceans*, vol. 108, no. C10, pp. 1–14, Oct. 2003.

[3] A. Stogryn, “The emissivity of sea foam at microwave frequencies,” *J. Geophys. Res.*, vol. 77, no. 9, pp. 1658–1666, Mar. 1972.

[4] M. D. Anguelova and P. W. Gaiser, “Dielectric and radiative properties of sea foam at microwave frequencies: Conceptual understanding of foam emissivity,” *Remote Sens.*, vol. 4, no. 5, pp. 1162–1189, Apr. 2012.

[5] Y. Quilfen, C. Prigent, B. Chapron, A. A. Mouche, and N. Houti, “The potential of QuikSCAT and WindSat observations for the estimation of sea surface wind vector under severe weather conditions,” *J. Geophys. Res.*, vol. 112, no. C9, Sep. 2007, Art. ID 01480227.

[6] N. Reul *et al.*, “SMOS satellite L-band radiometer: A new capability for ocean surface remote sensing in hurricanes,” *J. Geophys. Res. Oceans*, vol. 117, no. C2, pp. 1–24, Feb. 2012.

[7] L. H. Holthuijsen, M. D. Powell, and J. D. Pietrzak, “Wind and waves in extreme hurricanes,” *J. Geophys. Res. Oceans*, vol. 117, no. C9, pp. 1–15, Sep. 2012.

[8] S. Soisuvarn, Z. Jelenak, and W. L. Jones, “An ocean surface wind vector model function for a spaceborne microwave radiometer,” *IEEE Trans. Geosci. Remote Sens.*, vol. 45, no. 10, pp. 3119–3130, Oct. 2007.

[9] E. W. Uhlhorn *et al.*, “Hurricane surface wind measurements from an operational stepped frequency microwave radiometer,” *Monthly Weather Rev.*, vol. 135, no. 9, pp. 3070–3085, Sep. 2007.

[10] T. Meissner and F. J. Wentz, “The emissivity of the ocean surface between 6 and 90 GHz over a large range of wind speeds and earth incidence angles,” *IEEE Trans. Geosci. Remote Sens.*, vol. 50, no. 8, pp. 3004–3026, Aug. 2012.

[11] F. J. Wentz, “A model function for ocean microwave brightness temperatures,” *J. Geophys. Res.*, vol. 88, no. C3, pp. 1892–1908, Feb. 1983.

[12] C. Kummerow and R. Ferraro, *Algorithm Theoretical Basis Document: EOS/AMSR-E Level-2 Rainfall*. Fort Collins, CO, USA: Colorado State Univ. Rep., 2007, pp. 1–10.

[13] C. Surussavadee and D. H. Staelin, “Millimeter-wave precipitation retrievals and observed-versus-simulated radiance distributions: Sensitivity to assumptions,” *J. Atmos. Sci.*, vol. 64, no. 11, pp. 3808–3826, Nov. 2007.

[14] S. Y. Matrosov and E. M. Shulgina, “Scattering and attenuation of microwave radiation by precipitation,” *MGO Trans.*, vol. 448, pp. 85–94, 1982.

[15] L. M. Mitnik and M. L. Mitnik, “Retrieval of atmospheric and ocean surface parameters from ADEOS-II Advanced Microwave Scanning Radiometer (AMSR) data: Comparison of errors of global and regional algorithms,” *Radio Sci.*, vol. 38, no. 4, p. 8065, Aug. 2003.

[16] F. J. Wentz, “A well-calibrated ocean algorithm for special sensor microwave/imager,” *J. Geophys. Res.*, vol. 102, no. C4, pp. 8703–8718, Apr. 1997.

[17] H. J. Liebe and D. H. Layton, “Millimeter-wave properties of the atmosphere: Laboratory studies and propagation modeling,” Nat. Tech. Inf. Serv. Boulder, CO, USA, NTIA Rep. 87-24, 1987.

[18] D. D. Turner, M. P. Cadeddu, U. Lohnert, S. Crewell, and A. M. Vogelmann, “Modifications to the water vapor continuum in the microwave suggested by ground-based 150-GHz observations,” *IEEE Trans. Geosci. Remote Sens. Lett.*, vol. 47, no. 10, pp. 3326–3337, Oct. 2009.

[19] E. V. Zabolotskikh, L. M. Mitnik, and B. Chapron, “New approach for severe marine weather study using satellite passive microwave sensing,” *Geophys. Res. Lett.*, vol. 40, no. 13, pp. 3347–3350, Jul. 2013.

[20] E. Zabolotskikh, L. Mitnik, N. Reul, and B. Chapron, “New possibilities for geophysical parameter retrievals opened by GCOM-W1 AMSR2,” *IEEE J. Sel. Topics Appl. Earth Observ. Remote Sens.*, to be published. AQ2

[21] GCOM-W1 Data Providing Service Users Manual Jpn Aerosp. Exploration Agency, Tokyo, Japan, 2013.

[22] I. P. Mazin and A. K. Khrgian, *Clouds and Cloudy Atmosphere*. Leningrad, Russia: Gidrometeoizdat, 1989.

[23] B. A. Harper, J. D. Kepert, and J. D. Ginger, “Guidelines for converting between various wind averaging periods in tropical cyclone conditions,” World Meteorol. Org. TCP Sub-Project Rep., Geneva, Switzerland, 1555, 2010.

[24] B. Chapron *et al.*, “Ocean remote sensing data integration-examples and outlook,” in *Proc. OceanObs*, 2010, pp. 1–11.

IEEE Proof

AUTHOR QUERIES

AUTHOR PLEASE ANSWER ALL QUERIES

Please be aware that authors are required to pay overlength page charges ($200 per page) if the paper is longer than 3 pages. If you cannot pay any or all of these charges please let us know.

This pdf contains 2 proofs. The first half is the version that will appear on Xplore. The second half is the version that will appear in print. If you have any figures to print in color, they will be in color in both proofs.

The “Open Access” option for your paper expires when the paper is published on Xplore in an issue with page numbers. Papers in “Early Access” may be changed to “Open Access.”

AQ1 = Please check if the provided definition for GCOM-W1 here in the abstract and in the body of the text is correct, and please amend if necessary.

AQ2 = Please provide publication update in Ref. [20].

END OF ALL QUERIES

IEEE Proof